

PAPER • OPEN ACCESS

Evaluation of Gaussian wake models under different atmospheric stability conditions: Comparison with large eddy simulation results

To cite this article: Maria Krutova *et al* 2020 *J. Phys.: Conf. Ser.* **1669** 012016

View the [article online](#) for updates and enhancements.



240th ECS Meeting ORLANDO, FL

Orange County Convention Center **Oct 10-14, 2021**



Abstract submission due: April 9

SUBMIT NOW

Evaluation of Gaussian wake models under different atmospheric stability conditions: Comparison with large eddy simulation results

Maria Krutova, Mostafa Bakhoday Paskyabi, Finn Gunnar Nielsen, Joachim Reuder

Geophysical Institute, University of Bergen and Bergen Offshore Wind Centre, Bergen, Norway

E-mail: Maria.Krutova@uib.no

Abstract. The calculation of the velocity deficit in the wake of individual wind turbines is a fundamental part of the wind farm analysis. A good approximation of the wake deficit behind a single wind turbine will improve the power estimation for downwind turbines. Large-eddy simulation (LES) is a research tool widely used in studying the velocity deficit and turbulence intensity in the wake. However, the computational cost of the LES prevents its application in wind farm performance analysis and control. Existing analytical wake models provide a fast estimation of the velocity deficit and the wake expansion rate downstream from the rotor. The Gaussian wake models use a Gaussian distribution to improve the prediction of the wake velocity deficit. With the number of analytical models available, an extensive evaluation of their performance under different flow parameters is needed. In this work, we simulate a wake of a single wind turbine using the LES code PALM (Parallelized LES Model) combined with an actuator disc model with rotation. We compare the computed flow field with the predictions made by Gaussian models and fit their parameters to obtain the best possible fit for the wake field data as computed by LES.

1. Introduction

Inside a wind farm, the wind turbines are subjected to the influence of upstream turbines. The wake, an area with reduced mean velocity and increased turbulence intensity, is formed behind a working wind turbine due to the extraction of kinetic energy from the flow. Far downstream, the wake velocity eventually recovers to the free-flow velocity. However, the distances between wind turbines in a wind farm are usually shorter than needed for the full recovery. Therefore the wind turbines subjected to a wake operate under reduced wind speed. Since the available wind power is proportional to the cube of wind speed U^3 , it is crucial to predict the wake velocity deficit accurately.

Wake models range from simple analytical expressions to complex Computational Fluid Dynamic (CFD) codes. One of the latter, the large-eddy simulation (LES), is widely used in atmospheric boundary layer studies. LES resolves large turbulence scales directly and simulates subgrid scales and therefore is capable of handling turbulent flows such as wind turbine wakes. The LES can reproduce wake field characteristics in detail but requires grid resolution fine enough to resolve all turbulence scales of interest. The high-fidelity LES demands a significant amount of time and computational resources. Analytical wake models are less demanding but simplify



Content from this work may be used under the terms of the [Creative Commons Attribution 3.0 licence](https://creativecommons.org/licenses/by/3.0/). Any further distribution of this work must maintain attribution to the author(s) and the title of the work, journal citation and DOI.

the wake shape and wake velocity distribution. The simplest analytical models (Jensen [1], Frandsen [2]) assume a top-hat distribution of the wake deficit at each cross-section. A recent development in the analytical wake models, Gaussian models, suggests improving the wake-deficit distribution estimation by replacing the top-hat distribution with a Gaussian distribution.

In this study, we use the LES code PALM [3] to generate wind turbine wake fields at $U_\infty = 10$ m/s and 15 m/s. We then assign this data as an input field to four Gaussian models: Bastankhah & Porté-Agel [4], Jensen-Gaussian [5], Ishihara [6], and Double Gaussian [7] models. In Section 2, we briefly describe the models, their governing equations, special features, and select the parameters to fit the simulated wake field data. Section 3 introduces the LES code PALM and the configuration used to simulate a wind turbine wake under neutral and stable atmospheric conditions. We evaluate the parameters of Gaussian models by fitting them to various data slices of the LES wake flow fields. Applying fitted parameters, we compare the models' capability to predict the full LES wake and discuss the results in Section 4. We give a summary of the findings in Section 5.

2. Methodology

To calculate the wake field with an analytical wake model, we use the Cartesian coordinate system (x, y, z) centered at the foundation of a wind turbine so that the x -axis is aligned with the wind direction and z -axis is positive upwards.

The analytical wake models describe the wake velocity U_w or the normalized wake velocity deficit $\Delta U = 1 - U_w/U_\infty$ based on the following characteristics: downstream distance x from the turbine, wind turbine diameter D , and hub height z_h . Besides the wind turbine characteristics, the wake models also use the thrust coefficient C_T and the ambient turbulence intensity I_a estimated upwind of the rotor plane. Each model has one or more parameters to define the wake shape and/or expansion rate. The axisymmetric models regarded in this study implicitly assume that the wake does not interfere with the lower boundary, represented by the land or sea surface. The effect of vertical shear in the incident wind field is not considered.

2.1. Top-hat analytical models

While the top-hat analytical models are not the focus of this research, their concepts are borrowed and extended by the Gaussian wake models. Hence we provide a short description of the Jensen and Frandsen models.

2.1.1. The Jensen model [1] assumes linear expansion of a fully turbulent wake and equal velocity deficit in the cross-section of the wake (top-hat distribution). The expansion coefficient k defines the increase of the wake diameter D_w with the downstream distance x as follows

$$D_w(x) = D + 2kx. \quad (1)$$

The velocity deficit is calculated as

$$\Delta \bar{U} = \left(1 - \sqrt{1 - C_T}\right) \left(\frac{D}{D_w}\right)^2. \quad (2)$$

While several methods to define k are suggested, we use the one that allows linking wake expansion with ambient turbulence intensity: $k \approx 0.4I_a$ [8].

2.1.2. The Frandsen model [2] also assumes an equal velocity deficit in the cross-section of the wake but uses a different approach to calculate the wake diameter.

$$D_w(x) = D(\beta + \alpha \cdot x/D)^{1/2} \quad (3)$$

where the induction factor α is determined experimentally or corrected from the wake growth rate k in the Jensen model. The coefficient β is related to the thrust coefficient C_T by

$$\beta = \frac{1}{2} \cdot \frac{1 + \sqrt{1 - C_T}}{\sqrt{1 - C_T}}. \quad (4)$$

The wake deficit also depends on C_T and is calculated as follows

$$\Delta\bar{U} = \frac{1}{2} - \frac{1}{2} \sqrt{1 - 2 \left(\frac{D}{D_w} \right)^2 C_T}. \quad (5)$$

2.2. Gaussian wake models

The general form of a Gaussian wake model is given by

$$\Delta\bar{U} = A \cdot F(x, C_T, I_a) \cdot G(r, \sigma(x)) \quad (6)$$

where

- $\Delta\bar{U} = 1 - U_w/U_\infty$ is the normalized wake velocity deficit;
- A is an optional scaling constant;
- $F(x, C_T, I_a)$ is an amplitude function which defines the maximum normalized velocity deficit at the wake centerline;
- $G(r, \sigma(x))$ denotes a Gaussian function;
- $r^2 = y^2 + (z - z_h)^2$ is a radial coordinate;
- $\sigma = \sigma(x)$ is the standard deviation of a Gaussian function, defining the wake width.

2.2.1. The Bastankhah & Porté-Agel model, further referred to as BPA, exists in several formulations. In this study, we use the axisymmetric version of the model that includes ambient turbulence intensity [4].

The BPA model retains the linear expansion of the wake similar to the Jensen model (Eq. (1)) but introduces a different coefficient – the growth rate of the wake k^* – so that the standard deviation $\sigma(x)$ of the Gaussian distribution is

$$\frac{\sigma}{D} = k^* \frac{x}{D} + \varepsilon, \quad (7)$$

where the growth rate of the wake k^* is a linear function of turbulence intensity [4]:

$$k^* = 0.003678 + 0.3837I_a, \quad (8)$$

and ε can be expressed as $\varepsilon = 0.2\sqrt{\beta}$ [9], where β is defined in Eq. (4).

The normalized wake velocity is then given by the BPA model as

$$\Delta\bar{U} = \left(1 - \sqrt{1 - \frac{C_T}{8(\sigma/D)^2}} \right) \times \exp\left(-\frac{r^2}{2\sigma^2}\right). \quad (9)$$

In our study, we preserve the linear function as $k^* = k_1^* + k_2^*I_a$ where the parameters k_1^* and k_2^* are to be identified by fitting $\Delta\bar{U}$ to the simulation data.

2.2.2. *The Jensen-Gaussian model* [5] is a modification of the Jensen model.

The wake radius is calculated similarly to the Jensen model (Eq. 1) with the expansion coefficient k corrected for turbulence intensity:

$$r_x = r_1 + k_{wake}(k, C_T, I_a)x, \quad (10)$$

where $r_1 = r_d \sqrt{(1-a)/(1-2a)}$ is the original rotor radius corrected for the axial induction [5].

Furthermore, the top-hat distribution of the wake deficit is replaced by the Gaussian distribution to satisfy the following conditions:

- (i) 99% of the Gaussian distribution lies within the wake radius r_x (Eq. 10), i.e., the corresponding quantile for the Gaussian distribution is $z_{0.99} = 2.58$ from which the standard deviation should be $\sigma = r_x/2.58$.
- (ii) The wind velocity outside the wake radius r_x is set equal to the free stream velocity U_∞ .
- (iii) The model has the same mass flow as the Jensen model.

Applying the above assumptions will lead to the following expression for the normalized wake velocity deficit:

$$\Delta \bar{U} = \left[1 - \frac{5.16}{\sqrt{2\pi}} \cdot \bar{U}^*(x, k_{wake}(k, C_T, I_a)) \right] \times \exp\left(-\frac{r^2}{2\sigma^2}\right), \quad \sigma = r_x/2.58 \quad (11)$$

The exact definitions of functions $k_{wake}(k, C_T, I_a)$ and $\bar{U}^*(x, k_{wake})$ are omitted for brevity and can be found in the original study [5].

As seen from Eq. (10) and (11), the wake expansion coefficient k is included in the Jensen-Gaussian model through the function k_{wake} . The initial value of k is defined as in the Jensen model: $k = 0.4I_a$ (Section 2.1.1 and [8]).

2.2.3. *The Ishihara model* [6] proposes a general expression for the normalized velocity deficit of the full-wake:

$$\Delta \bar{U} = (a + b \cdot x/D + p)^{-2} \times \exp\left(-\frac{r^2}{2\sigma^2}\right). \quad (12)$$

The standard deviation σ is defined as in the BPA model Eq. (7). The coefficients k^* and ε are calculated from thrust coefficient C_T and ambient turbulence intensity I_a as given in [6]:

$$k^* = 0.11C_T^{1.07}I_a^{0.20}, \quad \varepsilon = 0.23C_T^{-0.25}I_a^{0.17}. \quad (13)$$

The coefficients a and b are in turn dependent on k^* and ε as

$$a = 4C_T^{-0.5}\varepsilon, \quad b = 4C_T^{-0.5}k^*. \quad (14)$$

The dimensionless coefficient p in Eq. (12) is expressed through another coefficient c as

$$p = \frac{c}{(1+x/D)^2}, \quad c = 0.15C_T^{-0.25}I_a^{-0.7}. \quad (15)$$

The coefficient p performs a near-wake correction for the amplitude function $F(x, C_T, I_a)$ (Eq. 6). The role of the correction coefficient is detailed further in Section 2.3.

According to Eq. (13) and (15), k^* , ε and c of the Ishihara model are represented as functions of C_T , I_a , and three tunable parameters for each function:

$$k^* = k_1C_T^{k_2}I_a^{k_3}, \quad \varepsilon = \varepsilon_1C_T^{\varepsilon_2}I_a^{\varepsilon_3}, \quad c = c_1C_T^{c_2}I_a^{c_3}. \quad (16)$$

Overall, there are nine parameters to be identified: k_1 , k_2 , k_3 , ε_1 , ε_2 , ε_3 , c_1 , c_2 and c_3 .

2.2.4. *The Keane Double Gaussian model* [7] extends the BPA model's approach to account for the two peaks often present in the wake measurements near the wind rotor:

$$\Delta\bar{U} = A \cdot F(\sigma(x), C_T) \cdot G(r, \sigma(x)). \quad (17)$$

The double Gaussian function $G(r, \sigma(x))$ describes the axisymmetric wake as

$$G(r, \sigma(x)) = \frac{1}{2} (e^{W_+} + e^{W_-}), \quad W_{\pm} = -\frac{(r \pm r_0)^2}{2\sigma^2(x)}, \quad (18)$$

where r_0 is the radial position of the extremum of a Gaussian function. For $r_0 = 0$, the function collapses to a single Gaussian function. For $r_0 > 0$, a double peak appears in a wake profile. The estimation $r_0 = 0.75D/2$, or 75% of the rotor radius, is suggested by the original study as a good approximation.

The standard deviation σ characterizes the width of each of the two Gaussian profiles as

$$\sigma(x) = k^* x^{1/3} + \varepsilon. \quad (19)$$

The Double Gaussian model does not include turbulence intensity I_a in the formulation, i.e., the amplitude function is expressed only by the standard deviation and the thrust coefficient as

$$F(\sigma(x), C_T) = \frac{M - \sqrt{M^2 - \frac{1}{2}N C_T D^2}}{2N}, \quad (20)$$

where erf is the error function and

$$\tau = r_0/\sigma, \quad (21)$$

$$M = 2\sigma^2 \exp\left(-\frac{1}{2}\tau^2\right) + \sqrt{2\pi}r_0\sigma[\text{erf}(\tau/\sqrt{2}) - 1], \quad (22)$$

$$N = \sigma^2 \exp(-\tau^2) + \frac{1}{2}\sqrt{\pi}r_0\sigma[\text{erf}(\tau) - 1]. \quad (23)$$

It should be noted that the original form of the Double Gaussian model probably has a typo in the expressions for M and N (page 3 in [7]). The expressions provided here are corrected according to the model output under default parameters compared to the original work.

In this study, we choose variables k^* , ε , and A as fitting parameters. Unlike the previous models, the Double Gaussian model does not have universal parameters. We select two sets of the original study parameters that correspond to free-flow speeds of 10 – 12 m/s and 16 – 18 m/s (Table 1 in [7], note that ε has to be additionally multiplied by the rotor diameter D). The selected parameters are used as initial guesses for the $U_{\infty} = 10$ m/s and $U_{\infty} = 15$ m/s simulations, respectively.

2.3. Overview of the Gaussian wake models

The characteristics of the Gaussian wake models are summarized in Table 1. The recommended parameters provided in the original formulation of each wake model are used as initial guesses for the fitting function and are further referred to as default parameters. All tunable parameters are constrained to a specific range to keep the values physically sensible and to avoid curve fitting failure.

The sample flow fields are calculated with each Gaussian model for the thrust coefficient $C_T = 0.763$ and turbulence intensity $I_a = 6.6\%$. The normalized velocity deficit distribution at the hub height $z_h = 102$ m is shown in Fig. 1.

Table 1. Gaussian wake models.

Model	# of parameters	Recommended values	I_a included
BPA (I_a)	2	$k_1^* = 0.003678, k_2^* = 0.3837$	Yes
Ishihara	9	Yes, see Eq. (13), (15)	Yes
Jensen Gaussian	1	$k = 0.4I_a$	Yes
Double Gaussian	3	N/A	No

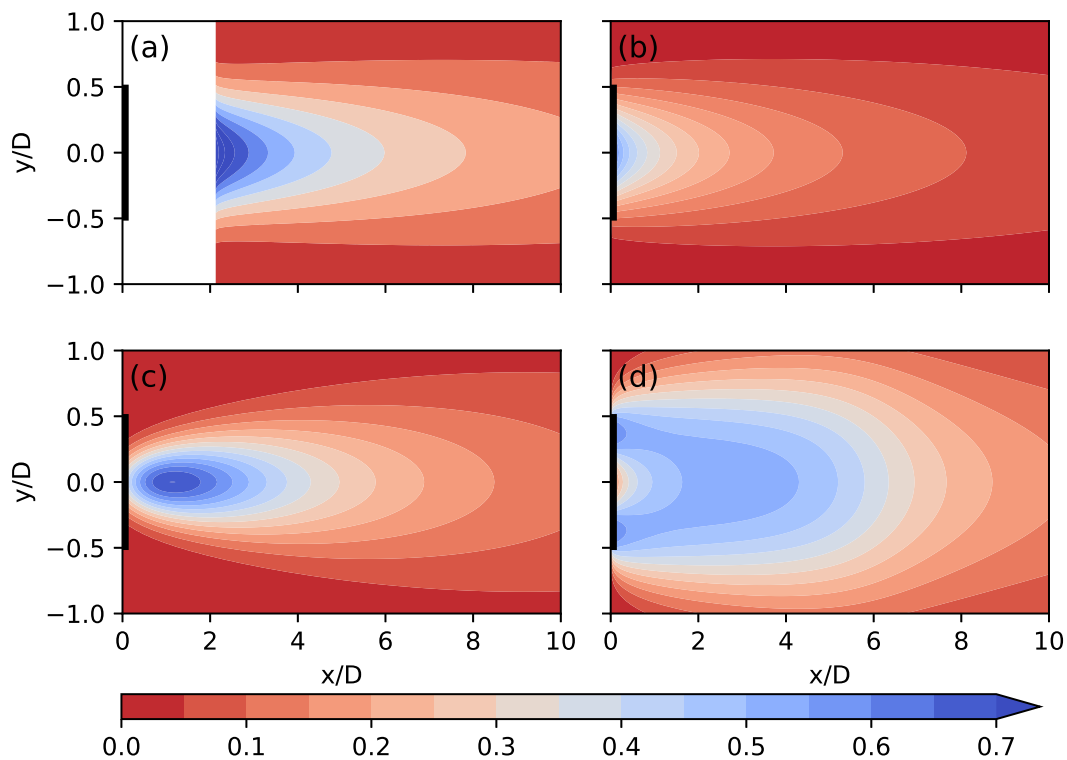


Figure 1. The normalized wake velocity deficit in a horizontal section at the hub height, calculated using Gaussian models with default parameters for $C_T = 0.763$, $I_a = 6.6\%$. (a) BPA, (b) Jensen-Gaussian, (c) Ishihara, (d) Double Gaussian

The BPA model (Fig. 1a) predicts a slowly expanding wake for the selected conditions. However, the BPA model cannot resolve a wake for $x/D \leq 2$ and high thrust coefficient because of the negative value under the square root $\sqrt{1 - \frac{C_T}{8(\sigma/D)^2}}$. Nevertheless, the unresolved region is not a critical flaw of the model, since the main interest is predicting wake influence on the downwind turbines.

The Jensen-Gaussian model (Fig. 1b) predicts a short near-wake. Without a comparison to a reference wake field, it is difficult to determine whether the initial guess of $k = 0.4I_a$ is correct or should be approximated better. Yet, it is possible to say that the Jensen-Gaussian model is rather sensitive to its only tunable parameter k . Decreasing k brings the wake growth rate closer to linear and delays wake recovery. Judging from the wake shape, it may be expected that the Jensen-Gaussian and the BPA models can give similar predictions as the parameters

k , and k_1^* and k_2^* are adjusted accordingly.

The Ishihara model (Fig. 1c) places a region of the high velocity deficit at $x/D \approx 1$. At the same time, the near-wake is narrower than predicted by other models. The far-wake grows slightly faster than in the BPA and Jensen-Gaussian models for the same conditions.

As follows from Eq. (12) the Gaussian function of the Ishihara model does not affect the velocity deficit at the centerline $r = 0$. Therefore, we can review the influence of the correction coefficient p on the centerline velocity deficit. An example amplitude function at the centerline is plotted in Fig. 2. Since p is inverse proportional to the normalized downstream distance x/D , the correction effect decreases with an increase of the downstream distance. As shown in Fig. 2, the coefficient p has a strong influence at the downstream distance $x/D \leq 2$. For $x/D \rightarrow \infty$, the value of p becomes negligible; the amplitude function with and without the correction coincide.

If no correction coefficient is present for the near-wake, i.e., $p = 0$ ($c = 0$) regardless of the downstream distance, the velocity deficit may exceed 1 near the center of the rotor. The velocity deficit $\Delta \bar{U} > 1$ corresponds to $U_w/U_\infty < 0$, or the wake velocity $U_w < 0$, i.e., reverse flow. Therefore, the coefficients p and c must be positive to avoid non-physical values of the velocity deficit in the near-wake.

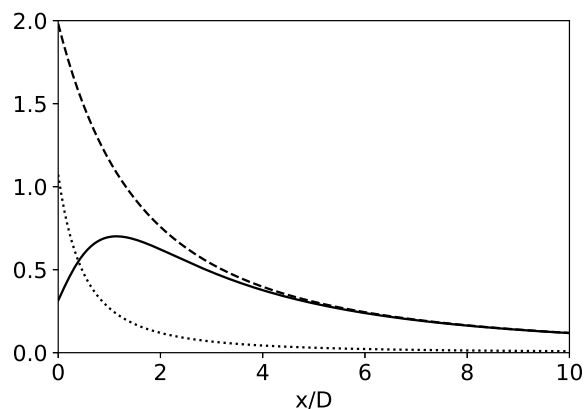


Figure 2. The effect of the near-wake correction on the amplitude function of the Ishihara model, calculated for NBL $U_\infty = 10$ m/s, $C_T = 0.763$, $I_a = 6.6\%$.

— amplitude function with a correction, - - - amplitude function without a correction, correction coefficient p .

The Double Gaussian model (Fig. 1d) stands out by predicting significantly larger wake width compared to other models. The parameter k^* of the Double Gaussian model affects the width of each of the Gaussian distributions. Decreasing k^* reduces the overall width of the wake but delays merging of the two profiles. Other parameters of the Double Gaussian model provide little effect on the predicted wake width.

3. PALM LES

3.1. Model description

PALM is an open-source Fortran LES code developed at the University of Hanover and capable of simulating turbulent atmospheric processes. The wind turbine simulation is performed using a supplementary module written by the research group from the University of Oldenburg. The module implements an actuator disk model with rotation (ADM-R) to simulate a wind turbine rotor [10]. The model is based on the concept suggested by Wu and Porté-Agel [11]. The original actuator disk model without a rotation (ADM) assumes a uniform distribution of the thrust force across the disc and does not consider the effect of turbine-induced rotation. ADM-R

includes rotation into the model to improve the predictions. In ADM-R, the actuator disc is first split into annular areas. The lift and drag forces in each area are calculated using the blade element momentum theory. Each blade element assumes a 2D airfoil of the corresponding blade section. As shown in [11], ADM-R improves the agreement with wind tunnel measurements compared to ADM, especially in the near-wake. Additionally, ADM-R performs comparably to a more complex actuator line model (ALM) [12]. The effect of the nacelle and the wind tower effect can be taken into account through the drag coefficients.

Comparisons with FINO1 lidar measurements [13][14] confirmed that ADM-R captures the features of a near-wake rather well and has a reasonable agreement on the width and velocity deficit value in the far-wake. For the full description of the current wind turbine model implementation, we refer to Section 3.7 of the PALM overview [3].

3.2. LES configuration

LES are carried out in PALM for a single NREL 5 MW wind turbine [15] with a diameter of $D = 126$ m and horizontal wind speed of $U_\infty = 10$ m/s (near rated) and 15 m/s (above rated) at the hub height $z_h = 102$ m. Two stability conditions are simulated for each wind speed: neutral boundary layer (NBL) and stable boundary layer (SBL). Offshore conditions are assumed by a roughness length of $z_0 = 0.0005$ m for all cases. The domain size and the grid resolution Δ are chosen in accordance with the existing PALM simulations of wind turbines for different atmospheric stabilities [16].

Each simulation consists of two stages: the precursor run to let the turbulence develop, and the main run using the precursor run as an input for the larger domain with one wind turbine (Table 2). The grid cell is stretched vertically to reduce the number of cells in the z -direction. The stretching factor of 1.04 is applied after reaching the height h_z above the surface. The maximum possible height of a grid cell is capped with a value twice of the original resolution Δ . The height of the boundary layer in each stability case remains lower than h_z .

The geostrophic wind velocity is one of the initialization parameters for LES. Since the simulations are performed at the latitude 54°N , a correction is introduced for the geostrophic wind components U_g and V_g to compensate for the Coriolis effect and obtain the required horizontal free-flow wind speed U_∞ at the hub height. The corrections depend on the stability conditions and are listed in Table 3. The lateral velocity of the free-flow at the hub height stays within $V_\infty < 0.05$ m/s and may cause a small deflection of the wake. An additional NBL simulation for $U_\infty = 10$ m/s is performed on a $\Delta = 4$ m grid to reduce deflection. Furthermore, the LES of NBL $U_\infty = 10$ m/s implies the simulation on a finer grid ($\Delta = 4$ m), while the LES of NBL $U_\infty = 15$ m/s is still performed on a coarser grid ($\Delta = 6$ m).

Table 2. Domain size.

Case	Δ , m	Precursor run, points	Main run, points	h_z
Stable	4	$384 \times 384 \times 160$	$1792 \times 384 \times 160$	500 m
Neutral	4	$576 \times 576 \times 160$	$2304 \times 576 \times 160$	500 m
Neutral	6	$384 \times 384 \times 192$	$1536 \times 384 \times 192$	800 m

All precursor runs start with the surface temperature of $T_s = 277$ K and the vertical temperature gradient 1 K/m. For the simulation of the stable conditions, the surface is cooled down at a constant rate. The cooling rate is chosen in a way to avoid low-level jets in the upper part of the rotor disk, as they are not a focus of this study. The cooling rate is listed in Table 3 along with other parameters specific to each run.

Table 3. Initialization parameters for LES.

Case	U_∞ , m/s	U_g , m/s	V_g , m/s	surface cooling rate, K/h
Neutral ($\Delta = 4$ m)	10	10.544	-2.614	-
Neutral ($\Delta = 6$ m)	10	10.539	-2.590	-
Neutral ($\Delta = 6$ m)	15	16.412	-4.130	-
Stable	10	10.584	-3.530	0.15
Stable	15	16.034	-5.769	0.25

Each precursor run takes approximately 5 days (NBL) or 30 hours (SBL) of simulation time to reach the steady-state representation of the flow field. The main run uses the temperature gradient and the velocity profile from the precursor run as starting values.

3.3. Comparison of analytical models with LES

In this study, we fit the analytical wake models using the least-squares to the 10-minute average of normalized wake deficit $\Delta\bar{U}$, which is calculated from PALM LES data. We consider the following data slices:

- (i) *cross-section profiles*: the analytical models are fitted to profiles at $x/D = 1, 2, \dots, 10$ in the xy -plane at hub height;
- (ii) *vertical profiles*: the analytical models are fitted to profiles at $x/D = 1, 2, \dots, 10$ in the xz -plane passing through the rotor center;
- (iii) *centerline*: the analytical models are fitted to the velocity deficit at the centerline, starting from $x/D = 0, 1$ and 4 for comparison;
- (iv) *xy -plane at hub height*: fitting to two-dimensional data is expected to provide higher accuracy and is used to evaluate the profile fits.

A sub-domain of length $20D$ and square cross-section $1.5 \times 1.5D$ centered at the wind rotor center is cut from the LES data for fitting with the Gaussian wake models. A coarse detection of wake shape is performed for the LES data to exclude occasional velocity fluctuations in the free-flow from the fitting process. We consider that a point belongs to the wake if the velocity at the point is lower than free-flow velocity by at least 2.5%, i.e., $\Delta\bar{U} < 0.025$.

4. Results

Based on the LES for NBL conditions at $U_\infty = 10$ m/s and $I_a = 6.6\%$ (Fig. 3a) we define three regions inside a wake: the near-wake ($x/D \leq 4$) where the wake deficit distribution is most complex, the middle wake ($4 < x/D \leq 7$), and the far-wake ($x/D > 7$) where the wake speed is recovering to the free-flow speed.

As seen from Fig. 3, the double peak in the near-wake velocity deficit is prominent for $U_\infty = 10$ m/s. In the case of higher free-flow velocity, $U_\infty = 15$ m/s, the velocity deficit distribution is closer to a single Gaussian throughout the wake. The wake deficit is slightly higher for SBL conditions than for NBL conditions at the same downstream distances. Overall, the stability conditions affect the wake shape less than the free-flow velocity magnitude. A small wake deflection may be observed, due to the free-flow not perfectly aligned with the x -axis after the Coriolis force correction is applied.

The thrust coefficient and the turbulence intensity calculated in each case are provided in Table 4. The thrust coefficient for NBL conditions at $U_\infty = 10$ m/s varies with grid cell size

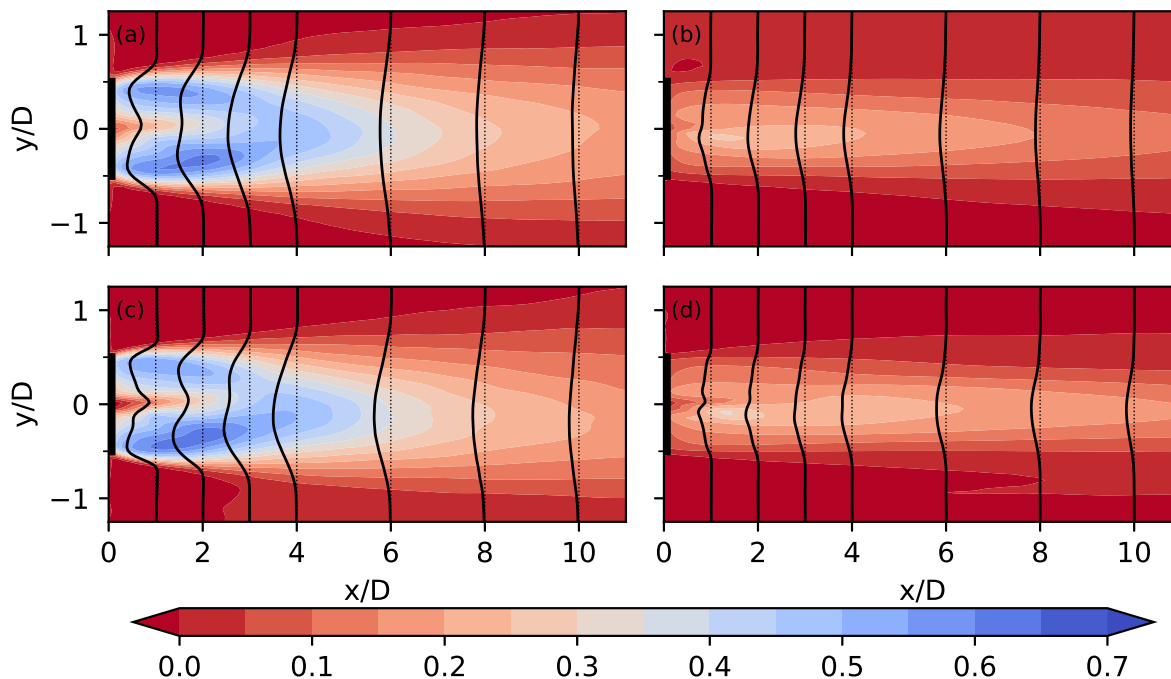


Figure 3. Normalized wake velocity deficit distribution $\Delta\bar{U}$ in the horizontal plane at hub height, LES 10-minute average. Solid lines mark the velocity deficit at selected distances x/D . The scale of the velocity deficit is the same for both plots. (a) NBL $U_\infty = 10$ m/s, (b) NBL $U_\infty = 15$ m/s, (c) SBL $U_\infty = 10$ m/s, (d) SBL $U_\infty = 15$ m/s.

due to the different number of grid points in the rotor area. The turbulence intensity is almost unaffected by the grid cell size.

Table 4. Flow parameters at $z_h = 102$ m from the LES data.

Case	U_∞ , m/s	C_T	I_a
Neutral ($\Delta = 4$ m)	10	0.763	6.6%
Neutral ($\Delta = 6$ m)	10	0.713	6.5%
Neutral ($\Delta = 6$ m)	15	0.205	5.8%
Stable	10	0.725	7.4%
Stable	15	0.217	4.3%

The models are compared based on how well they predict the wake in the hub height plane after the fitting. The results are provided in Tables 5–8 based on the lowest RMSE for a wake calculated in the hub height plane with the fitted parameters. The best fit out of profiles and centerline fits is marked in bold. In case of equal RMSEs with respect to round up to the fourth digit, the fit to a cross-section profile is given a priority. Fits to the horizontal plane at the hub height (column "HH plane" in tables) are performed only as a reference and are not considered in a comparison between best fits. As can be seen, identifying model parameters on a limited data set may show the results comparable to the fitting to two-dimensional data.

The BPA model returns an incorrect fit to the hub height plane for $U_\infty = 10$ m/s, as the model cannot resolve the wake at $x/D \leq 2$ for a high thrust coefficient. This fit is not included in Tables 5–6.

Table 5. Best fits for NBL and $U_\infty = 10$ m/s. RMSE is calculated for the wake in the horizontal plane at hub height using the fitted parameters.

Fitted to:	cross-section profile		vertical profile		centerline		HH plane	Default
Model	x/D	RMSE	x/D	RMSE	x/D	RMSE	RMSE	RMSE
BPA	9	0.0316	9	0.0311	4	0.0325	N/A	0.0428
Jensen-Gaussian	10	0.0784	10	0.0786	4	0.0785	0.0784	0.0864
Ishihara	2	0.1194	2	0.1192	4	0.0731	0.0662	0.0951
Double Gaussian	7	0.0814	6	0.0667	0	0.0622	0.0603	0.0757

Table 6. Best fits for SBL and $U_\infty = 10$ m/s. RMSE is calculated for the wake in the horizontal plane at hub height using the fitted parameters.

Fitted to:	cross-section profile		vertical profile		centerline		HH plane	Default
Model	x/D	RMSE	x/D	RMSE	x/D	RMSE	RMSE	RMSE
BPA	6	0.0382	5	0.0384	4	0.0390	N/A	0.0489
Jensen-Gaussian	2	0.0844	8	0.0844	4	0.0845	0.0844	0.0940
Ishihara	2	0.1155	2	0.1106	0	0.099	0.0728	0.0904
Double Gaussian	7	0.0909	6	0.0646	0	0.0644	0.0627	0.0742

Table 7. Best fits for NBL and $U_\infty = 15$ m/s. RMSE is calculated for the wake in the horizontal plane at hub height using the fitted parameters.

Fitted to:	cross-section profile		vertical profile		centerline		HH plane	Default
Model	x/D	RMSE	x/D	RMSE	x/D	RMSE	RMSE	RMSE
BPA	4	0.0181	4	0.0181	4	0.0181	0.0181	0.0274
Jensen-Gaussian	10	0.0241	10	0.0241	1	0.0244	0.0241	0.0369
Ishihara	2	0.0154	10	0.0154	0	0.0171	0.0140	0.0160
Double Gaussian	2	0.0322	3	0.0538	0	0.0474	0.0320	0.0856

4.1. Fitting to velocity deficit profiles

The velocity deficit distribution in the horizontal plane at hub height provides the essential information on the wake shape. The cross-section profiles in the horizontal plane are usually

Table 8. Best fits for SBL and $U_\infty = 15$ m/s. RMSE is calculated for the wake in the horizontal plane at hub height using the fitted parameters.

Fitted to:	cross-section profile		vertical profile		centerline		HH plane	Default
Model	x/D	RMSE	x/D	RMSE	x/D	RMSE	RMSE	RMSE
BPA	5	0.0240	6	0.0240	1	0.0240	0.0240	0.0309
Jensen-Gaussian	10	0.0242	10	0.0245	1	0.0238	0.0236	0.0394
Ishihara	9	0.0212	4	0.0216	1	0.0184	0.0168	0.0194
Double Gaussian	3	0.0401	1	0.0658	0	0.0608	0.0402	0.0888

close to symmetric and can be fitted with a Gaussian wake model. The velocity profiles in the vertical plane are affected by surface friction. We account for the wind shear by subtracting the averaged free-flow profile $U_\infty(z)$ from the vertical wake profile. We then fit the resulting profile with a Gaussian wake model.

The models split into two groups. The BPA and Jensen-Gaussian models fit the far-wake rather well and are further referred to as far-wake models. For each of these models, the coefficients obtained from fitting to any profile in the far-wake ($x/D > 7$) have a good agreement from case to case and show little differences in the RMSE. For the BPA model, the best fit may also be found in the middle wake ($4 < x/D \leq 7$). The RMSE returned by the BPA model is always lower by half compared to the RMSE of the Jensen-Gaussian model for the same far-wake profile-fit combination.

The other two models (Ishihara and Double Gaussian), further referred to as full-wake models, perform worse during the profile fitting. Both models aim to describe the near-wake's particular features: the high velocity deficit at the centerline (Ishihara) or the double peak in the velocity deficit cross-section profiles (Double Gaussian). Fitted to a single profile, they lack the information on the wake structure and return high RMSE.

Fitting the Ishihara model to a single velocity deficit profile sets the coefficient c and, consequently, the near-wake correction p to zero (Eq. 15). This result suggests that the model regards the whole wake as a far-wake when it receives the information on the velocity deficit of a single cross-section profile. The Ishihara model fitted to a near-wake profile overestimates the wake velocity in the far-wake. When fitted to a far-wake profile, the Ishihara model predicts negative velocity values (i.e. reverse flow) with an RMSE up to 0.5 in the near-wake.

The Double Gaussian model fitted to a near-wake profile captures the double peak well. The double peaks are also present in the far-wake, and the predicted velocity deficit is noticeably high for downstream distances $x/D \geq 7$. Fitting the Double Gaussian model to a far-wake profile improves the full-wake's prediction as reflected by best fits in Tables 5–8. In this case, the double peak is still predicted for the near-wake, although the wake velocity deficit is underestimated compared to LES. The RMSE for the near-wake cross-sections is comparable to the corresponding RMSEs of single Gaussian models (BPA and Jensen-Gaussian).

Full-wake models perform better in the case of strong wind, when the wake shape is smoother, and show an improvement of RMSEs compared to default parameters.

4.2. Centerline fitting

Fitting to the rotor centerline is essentially the fitting of an amplitude function of a Gaussian wake model. The centerline wake velocity deficit predicted by the LES has a convex shape (concave for the wake velocity), which lies in the $0 \leq x/D \leq 4$ range (Fig. 4a). The convexity

is especially emphasized for $U_\infty = 10$ m/s. This shape provides a challenge for far-wake models (BPA, Jensen-Gaussian) that assume monotonic recovery of the wake velocity. Besides $x/D \geq 0$ fit (entire centerline), we perform two supplementary fits to the partial centerline. A fit to the centerline segment $x/D \geq 1$ imitates missing data in the very near-wake area (centerline with data loss). A different fit to the segment $x/D \geq 4$ allows comparing the performance of the far-wake models (monotonic segment fit).

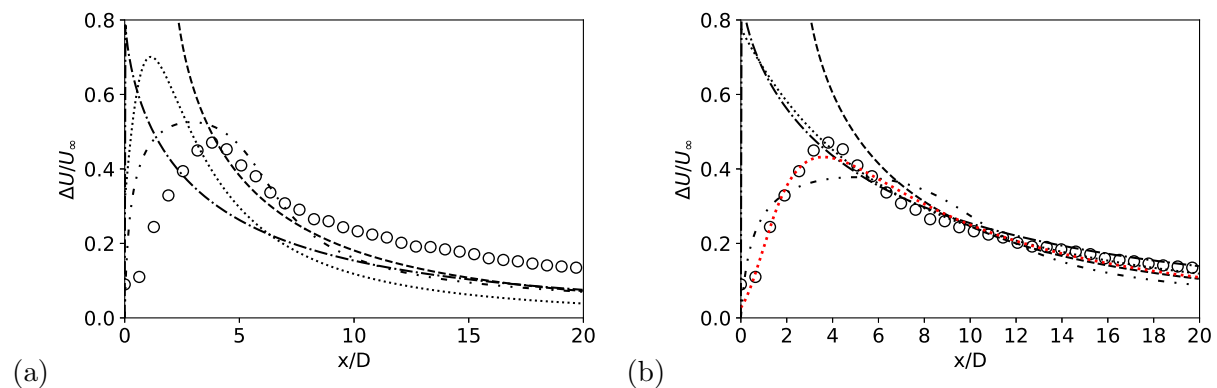


Figure 4. Normalized wake velocity deficit at the rotor centerline for NBL conditions with $U_\infty = 10$ m/s. (a) Default parameters, (b) Best overall fits to 10-minute average according to Table 5. \circ – LES data, - - - BPA, — · — Jensen-Gaussian, ····· Ishihara, ·····(red) Ishihara for $x/D \geq 0$, — · · — Double Gaussian

As seen from Tables 5–8, far-wake models tend to have the best fit for a part of the centerline segment, starting from $x/D \geq 4$. The parameters fitted to the monotonic centerline segment and the RMSE are close to the ones obtained from best fits to profiles.

Full-wake models (Ishihara, Double Gaussian) capture the centerline velocity profile’s features more precisely. In general, fitting full-wake models to the entire centerline or the centerline with data loss returns noticeably different parameters, but rather close RMSEs for single profiles and horizontal wake. Fitting full-wake models to the monotonic segment usually increases RMSE for near-wake profiles.

The Ishihara model may show low RMSE when fitted to the monotonic section. In this case, the fitted model predicts an extremely high velocity deficit in the near-wake (Fig. 4) and sets the near-wake coefficient p to zero. At the same time, the full centerline fit returns comparable RMSE for the Ishihara model, but completely different parameters. Therefore, the RMSE criterion alone is not enough to identify the best fit for the Ishihara model.

The Double Gaussian model improves its accuracy when fitted to the centerline at $U_\infty = 10$ m/s and shows RMSE close to the control fit to the horizontal plane at hub height. Nevertheless, the Double Gaussian significantly overestimates the wake width and velocity deficit.

The comparison of cross-section profiles of velocity deficit in the far-wake at $x/D = 8$ is presented in Fig. 5 for NBL conditions with $U_\infty = 10$ m/s. The predictions calculated with default parameters underestimate the wake velocity deficit (Fig. 5a). The default BPA model has the closest match in terms of wake shape and deficit value. After the fitting (Fig. 5b), the BPA model follows the LES data most precisely but overestimates the centerline velocity deficit more than the Jensen-Gaussian and Ishihara models.

The parameters of each Gaussian model are identified for a 10-minute average velocity field. We provide best fits to a 1-hour average velocity field for NBL conditions with $U_\infty = 10$ m/s for comparison (Fig. 5c). For a 1-hour average velocity field, the maximum wake deficit at $x/D = 8$

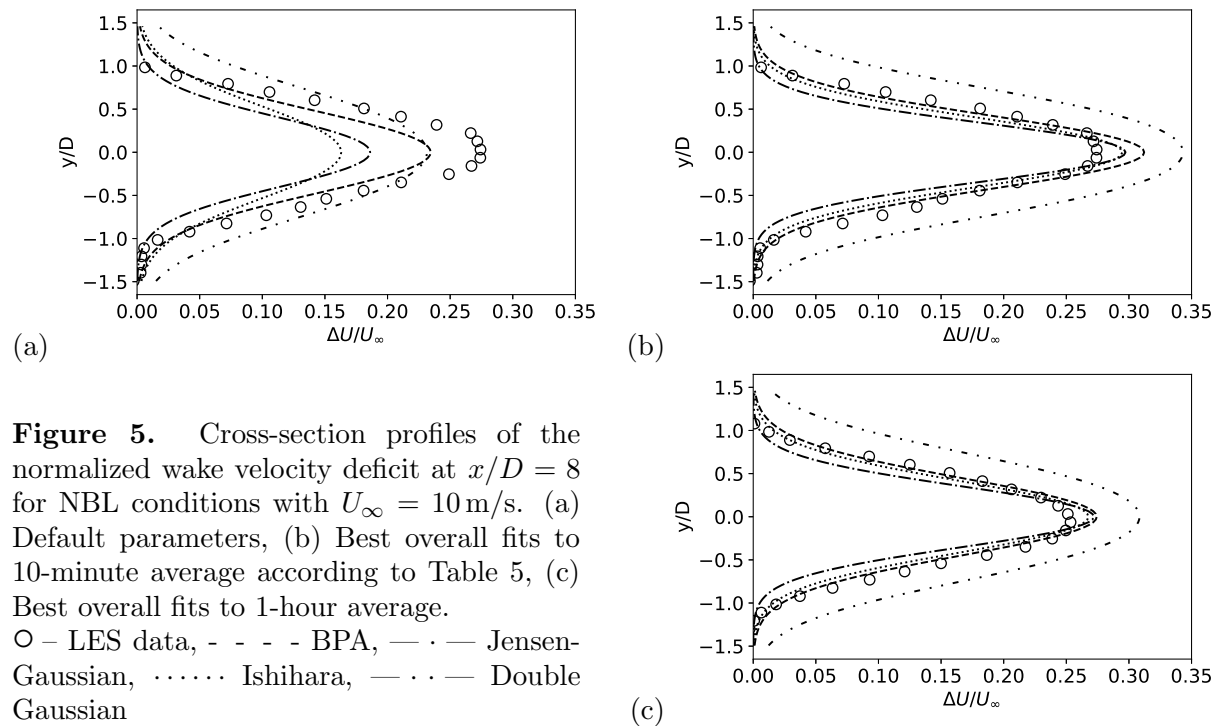


Figure 5. Cross-section profiles of the normalized wake velocity deficit at $x/D = 8$ for NBL conditions with $U_\infty = 10$ m/s. (a) Default parameters, (b) Best overall fits to 10-minute average according to Table 5, (c) Best overall fits to 1-hour average. \circ – LES data, - - - BPA, — · — Jensen-Gaussian, ····· Ishihara, — · — Double Gaussian

slightly decreases; all models except for the Double Gaussian show good agreement between LES data and each other.

In the case of SBL conditions with $U_\infty = 15$ m/s (Fig. 6), the Double Gaussian model shows the highest discrepancy between the LES wake before and after fitting. Other models, particularly the Ishihara model, have a better agreement.

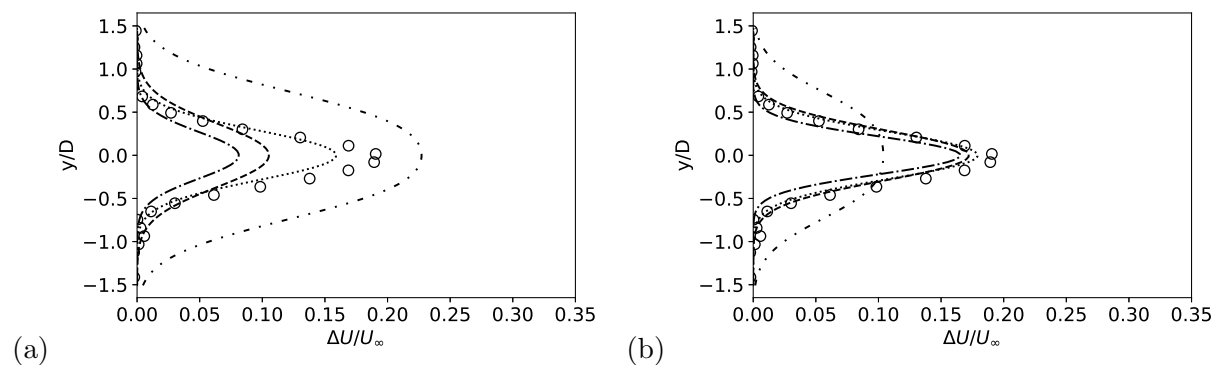


Figure 6. Cross-section profiles of the normalized wake velocity deficit at $x/D = 8$ for SBL conditions with $U_\infty = 15$ m/s. (a) Default parameters, (b) Best overall fits according to Table 8. \circ – LES data, - - - BPA, — · — Jensen-Gaussian, ····· Ishihara, — · — Double Gaussian

The Double Gaussian model is the only one among the regarded models which fully parametrizes the standard deviation. Therefore, it does not depend on the flow characteristics directly. It may be one of the reasons the model often overestimates the wake width compared to the one predicted by the LES and the other Gaussian wake models. A recent paper on the Double Gaussian model pointed out the momentum conservation issues of the original model and suggested a modification to resolve them [17].

5. Conclusion

Our main objective was a model-based study. We attempted to fit analytical models to the simulated data and observed their behavior. The comparison with observations is beyond the scope of this paper and will be performed in another independent research study.

In this study, we classified Gaussian wake models into two groups. We showed that the far-wake models (BPA, Jensen-Gaussian) did not accurately describe the near-wake, but they performed well in the far-wake. Both far-wake models showed a good agreement with the LES far-wake.

The full-wake models (Ishihara, Double Gaussian) attempt to describe the whole wake. When fitted to a single profile, they often do not predict the structure of the wake correctly. In some cases, fitting a full-wake model to the wind turbine centerline improved the predictions and gave RMSE comparable to the map fit to the horizontal plane at the hub height. Best fits for the BPA and Ishihara models usually followed the shape of the LES wake rather closely; the Jensen-Gaussian model predicted narrower width than the other models, but still got the wake shape right. Nevertheless, there was always a discrepancy between the peak deficit in a profile predicted by the LES and Gaussian models. The Double Gaussian model showed the worst agreement with the LES data compared to other models.

Considering that the far-wake approximation possesses more interest in wind farm applications, the use of far-wake models at the cost of the unresolved or poorly resolved near-wake can be justified.

Acknowledgments

The simulations were performed on resources provided by UNINETT Sigma2 - the National Infrastructure for High Performance Computing and Data Storage in Norway.

References

- [1] Jensen N O 1983 *A note on wind generator interaction*, (Roskilde: Risø National Laboratory)
- [2] Frandsen S, Barthelmie R J, Pryor S C, Rathmann O, Larsen S, Højstrup J and Thøgersen M 2006 *Wind Energy* **9**(1–2) 39–53
- [3] Maronga B et al 2020 *Geosci. Model Dev.* **13**(3) 1335–1372
- [4] Niayifar A and Porté-Agel F 2016 *Energies* **9**(9) 1–13
- [5] Gao X, Yang H and Lu L 2016 *Appl. Energy* **174** 192–200
- [6] Ishihara T and Qian G-W W 2018 *J. Wind Eng. Ind. Aerodyn.* **177** 275–292
- [7] Keane A, Aguirre P E O, Ferchland H, Clive P and Gallacher D 2016 *J. Phys.: Conf. Series.* **753**(3) 32–39
- [8] Göçmen T, Van Der Laan P, Réthoré P-E, Diaz A P, Larsen G C and Ott S 2016 *Renew. Sustain. Energy Rev.* **60** 752–769
- [9] Bastankhah M and Porté-Agel F 2014 *Renew. Energy* **70** 116–123
- [10] Dörenkämper M, Witha B, Steinfeld G, Heinemann D and Kühn M 2015 *J. Wind Eng. Ind. Aerodyn.* **144** 146–153
- [11] Wu Y-T and Porté-Agel F 2011 *Boundary-Layer Meteorology* **138**(3) 345–366
- [12] Porté-Agel F, Wu Y-T, Hao L and Conzemius R J 2011 *J. Wind Eng. Ind. Aerodyn.* **99**(4) 154–168
- [13] Vollmer L et al. 2015 *J. Phys.: Conf. Series.* **625**(1) 012001
- [14] Vollmer L, Steinfeld G and Kühn M 2017 *Wind Energy. Sci.* **2**(2) 603–614
- [15] Jonkman J, Butterfield S, Musial W and Scott G 2009 *Definition of a 5-MW Reference Wind Turbine for Offshore System Development* (USA: National Renewable Energy Laboratory)
- [16] Witha B, Steinfeld G, Dörenkämper M and Heinemann D 2014 *J. Phys.: Conf. Series.* **555** 012108
- [17] Schreiber J, Balbaa A, and Bottasso C L 2020 *Wind Energy. Sci.* **5**(1) 237–244